JOURNAL OF GEOPHYSICAL RESEARCH, VOL. 114, F01022, doi:10.1029/2007JF000913, 2009

Click Here for Full Article

Dry snow slab quasi-brittle fracture initiation and verification from field tests

D. M. McClung[1]

Received 24 September 2007; revised 19 September 2008; accepted 24 December 2008; published 24 February 2009.

[1] Dry snow slab avalanches initiate from shear fracture in a thin weak layer underneath a planar slab of cohesive snow. In this paper, field data from more than 400 snow shear fracture tests are analysed and applied to the problem of snow slab release and snow pack instability evaluation. The paper contains a new, but simple, analytical model to estimate the critical length for fracture. The model contains the assumption of a finite fracture process zone which may be a significant fraction of the slab depth D or the critical length L for weak layer shear fracture. The results suggest that the ratio L/D is of order 1 for both the data and the model as previously predicted for the snow slab. Using a combination of experimental results from laboratory tests, two sets of field data and the new model, suggests that previous theoretical arguments about snow slab release over almost 30 years are congruent with the field data. Simple extension to explain viscoelastic temperature effects and slope normal weak layer deformation on snow slab instability evaluation is included in the analysis. Since the experimental field data contain viscoelastic effects and slope normal effects, it is imperative to account for these in the model and for snow slab instability evaluation.

Citation: McClung, D. M. (2009), Dry snow slab quasi-brittle fracture initiation and verification from field tests, *J. Geophys. Res.*, *114*, F01022, doi:10.1029/2007JF000913.

1. Introduction

[2] Dry snow slab avalanches initiate by propagating shear fractures from within a thin relatively weak layer underneath a thicker, stronger slab. It has been known for 30 years [*McClung*, 1977] that alpine snow is a pressure sensitive, dilatant, strain-softening material when it fails in shear. The fundamental process involves the failure of bonds between grains which are a significant fraction of a millimeter size or more. The large failure elements (e.g., millimeter size) and the strain-softening behavior imply that the zone over which shear failure is taking place (called the fracture process zone (FPZ)) must be large and comparable to some important slab dimensions such as the slab depth, D, to measured perpendicular to the weak layer [*Bažant et al.*, 2003]. Thus, the fracture process zone is finite and it has been suggested that alpine snow is a quasi-brittle material [*McClung*, 1979, 1981; *Bažant et al.*, 2003] with a fracture mechanical size effect needed to explain the known decrease of nominal strength with increasing sample size. Up to now, since the fundamental paper by *Palmer and Rice* [1973] introducing quasi-brittle fracture mechanics to the Earth materials (soil, rock, snow, ice), most evidence for the Earth materials has come from laboratory tests instead of field tests to get the fundamental fracture characteristics. The exception, being the work of *Dempsey et al.* [1999] on ice. In this paper, I provide partial verification for the snow slab using the results of 488 fracture tests from field tests on alpine snow by *Gauthier and Jamieson* [2008], *Sigrist* [2006], and my own field measurements taken in March 2008. The field tests show that the median of the critical length ratio L/D, is $O(1)$ as predicted by [*Bažant et al.*, 2003].

[3] Since the experimental results show that the critical length, L, is comparable to slab depth, I also provide a simple one-dimensional model based on the work of *Cleary and Rice* [1974] which is applicable when the fracture process zone length, ω, is as large as the critical length ($\omega/L \leq 1$). The model allows theoretical estimates of the critical length in terms of slab and weak layer mechanical properties including pressure sensitivity which is a known characteristic of alpine snow [*McClung*, 1977, 1987; *McClung and Schaerer*, 2006]. The model contains the prediction that shorter critical lengths are expected for higher applied normal stress which is evident in the field tests of *Gauthier and Jamieson* [2008] and my tests in the winter of 2008. In addition, maximum estimates of ω are provided from the model and it is suggested that ω is $O(100)x\overline{E}$ as hypothesized by *McClung and Schweizer* [2006], where $\overline{E}$ is the mean grain size in the weak layer.

[4] In this paper, previous results obtained by *Palmer and Rice* [1973] and *Bažant et al.* [2003] are utilized but two extensions of their work are included. These extensions include the one dimensional model described above for ω comparable to L and provision for slope normal deformation within the fracturing weak layer which accompanies slope parallel shear deformation. The latter is described both in

[1]Department of Geography, University of British Columbia, Vancouver, British Columbia, Canada.

Copyright 2009 by the American Geophysical Union.
0148-0227/09/2007JF000913$09.00

Figure 1a. Photo of snow slab fractures with collapse (slope normal) deformation in the weak layer. A shear fracture propagated first up the low angled slope within the weak layer followed by tensile fracture through the slab initiated at the interface between collapsed and noncollapsed portions of the weak layer. Photo courtesy of the Department of Civil Engineering, University of Calgary, Calgary, Alberta, Canada.

laboratory tests and from field tests. Figure 1a shows a shear fracture which has propagated under a snow slab on a slope with slope normal deformation (collapse) prior to tensile fracture through the slab. Figure 1a suggests that the tensile fracture initiated from the bottom of the slab. The shear fracture in the weak layer propagated first with tensile fracture initiating at the interface between the collapsed and noncollapsed portion of the weak layer. Figure 1b shows a similar pattern from field tests on flat terrain (slope angle 0°) described below. In Figure 1b, the propagating shear fracture initiated at the point where the saw blade was turned upward with tensile fracture through the slab after a short propagation distance. Given that the shear fracture propagated along the weak layer, I suggest that a portion of the gravitational energy released by making the saw cut in the weak layer resulted in horizontal slip to drive the shear fracture in the weak layer. Figures 1a and 1b provide the motivation for simple extension of the previous work to account for the combination of slope normal and slope parallel deformation with a weak layer of finite thickness when it fractures.

[5] The quantitative aspects of the field fracture tests reported in this paper also confirm the importance of accounting for the normal stress effects implied by the new model. In this paper, the new model is presented first, followed by comparison with the fracture data from the field tests. The field tests do not contain all the material input needed so the comparison relies upon data from laboratory tests, including slab modulus and strain-softening data from shear fracture tests, as well as weak layer fracture energy determined from slab avalanche data. Since the data needed come from diverse sources, comparison of data with the theory is not highly precise but this is a common characteristic of field measured geophysical experiments.

2. Description of Field Tests and Characteristics of Data

[6] *Sigrist* [2006] and *Gauthier and Jamieson* [2008] provide detailed descriptions of the field tests used in this paper. The reader is referred to their work for more detail but a brief description is given here. The procedure involves introducing a cut upslope or downslope within a weak layer underneath a long rectangular block of snow cut free on all sides. The cut is made to a length L at which the shear fracture propagates rapidly within the weak layer. Figure 2 contains a schematic of the test setup. The block of snow is about 30 cm wide with a total length, L_0, ideally at least 3–

Figure 1b. Photo of fractures observed in field tests on horizontal terrain (slope angle 0°). The shear fracture initiated at the position where the saw is located by cutting through the weak layer from left to right. Tensile fracture through the slab occurred after the shear fracture propagated for about 20 cm. Photo courtesy of R. Burrows.

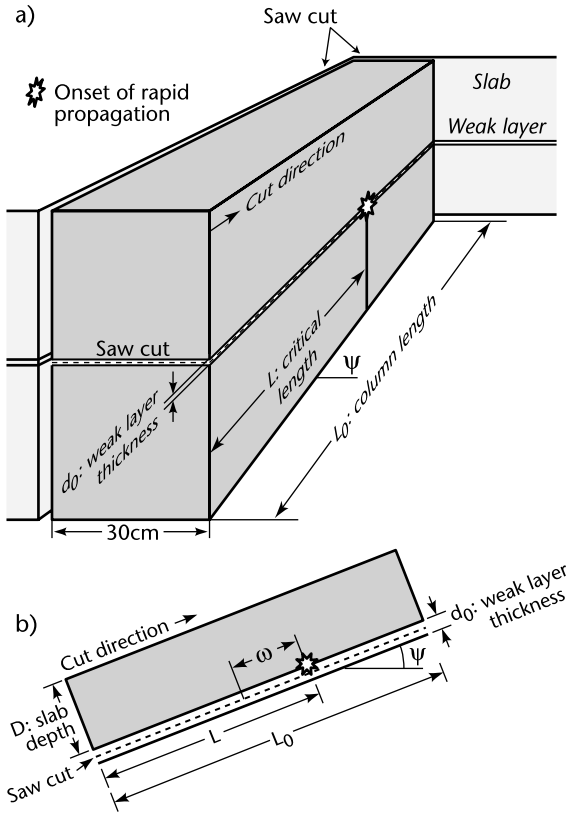

Figure 2. (a) Schematic for field tests made with a saw cut of critical length, L, within a weak layer of thickness, d_0, with a total block length, L_0, with slope angle ψ. (b) Side view schematic of the field tests with D as the slab depth. The parameter ω is the length of the fracture process zone. The coordinate system is defined such that x is measured from the left end of the block ($x = 0$) to the end of the cut or slip surface ($x = L$) in the direction of the dotted line in the center of the weak layer.

4 times the depth. In most of the tests, both ends of the block are cut free so that they represent free surfaces on the upslope and downslope ends and the sides of the block are also free surfaces. The cut within the weak layer is made either upslope from the lower end of the block or downslope from the upper end of the block. *Gauthier and Jamieson* [2008] showed that there is no statistical difference between cuts made upslope or downslope. For the remainder of this paper and in the model developed later, I will take the cut as being made upslope. *Gauthier and Jamieson* [2008] also performed tests for slopes of different angle from $\psi = 0°$–$50°$ (mean 25°) which provide evidence of normal stress and slab stiffness. My own data further clarify these effects, as shown below.

2.1. Length Scales in the Problem

[7] There are a number of length scales in the problem (Figure 2) including L_0, length of the block tested; L, critical length of the cut in the weak layer; D, slab depth measured perpendicular to the weak layer; ω, length of the fracture process zone for the shear crack or shear band; d_0, thickness of the weak layer; $\overline{E}$ mean size of grains in the weak layer; and $\overline{\delta}$, mean displacement during strain softening shear fracture for alpine snow. Table 1 gives some typical values and scaling ratios for these quantities. It is important to note that two of these quantities (ω, $\overline{\delta}$) are not measurable along with the field tests. Both quantities are connected from theoretical estimates provided by *Palmer and Rice* [1973] and also with a simple theoretical model explained below. The estimate of $\overline{\delta}$ comes from laboratory measurements of shear fracture of alpine snow. Thus, even though a theoretical explanation of the field tests requires all of the length scales above, it is important to recognize that not all of these can be measured with the field tests so that an explanation of the tests will require more input than is actually measured.

[8] In this paper, the terms shear crack, shear band and slip surface are taken to mean the same thing. In accordance with shear failure of alpine snow and other geotechnical materials they imply relative sliding within the weak layer. Also, the "crack" is not traction free but instead, there is frictional sliding with a relationship between shear stress, τ, and relative sliding displacement, δ. Acoustic emissions measured during simple shear experiments [*McClung*, 1987] show a sharp peak in emission rate prior to achievement of peak stress with rapid decline during softening. These experiments suggest there is considerable dilational straining and microfracturing prior to peak with formation of a slip surface at or slightly after peak stress. In the simple model below, it is assumed that sliding begins at peak stress with softening to residual stress after a mean displacement $\overline{\delta}$ whose magnitude is determined from laboratory fracture tests on alpine snow as about 0.1 mm. After residual stress in achieved, it is assumed that sliding takes place relative to surfaces of the band with τ at the residual value, τ_r.

Table 1. Length Parameters for Dry Snow Slab Avalanche Initiation and for the Test Data Used

Length Scale	Typical Values	Comments
L_0	0.2–2 m	Does not appear in the theory if $L_0/L \gg 1$.
L	0.07–0.95 m	Critical length ratio L/D is important in the theory and of great practical importance.
D	0.1–1.3 m	Fundamental scaling parameter for size effects in nominal shear strength and critical length ratio.
ω	5 to several 10s of cm	A material property scaled with grain size in Appendix A.
d_0	1 mm to several cm	If d_0 exceeds several mm or several times the mean grain size, vertical displacement (collapse) may take place in the FPZ.
$\overline{E}$	0.2–10 mm	Here ω is scaled with median values of E for weak layer types in Appendix A.
$\overline{\delta}$	0.1–0.3 mm	Fundamental parameter in the theory. The values come from fracture tests with rapid strain softening in lab tests.

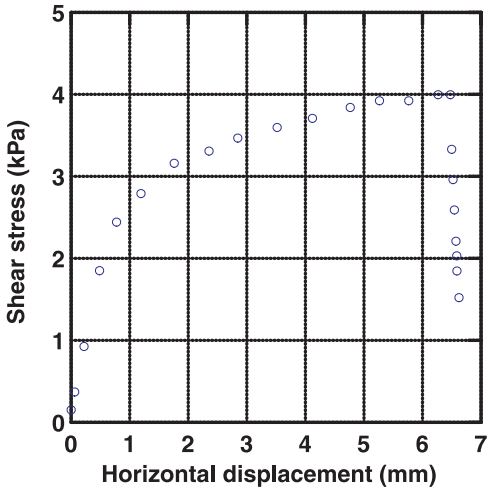

Figure 3a. Direct simple shear results for shear stress (kPa) versus horizontal displacement for faceted snow. Density is 165 kg/m^3, test temperature is −15°C, and grain size is 0.2–0.5 mm. The mean displacement by strain softening after peak stress is $\overline{\delta} \approx 0.1$ mm.

[9] In the case of the field tests, the saw cut induces both slope normal and slope parallel deformation and the cut may be envisioned as a crack with residual friction on the crack surfaces. In laboratory tests, straining and microcracking produces a slip surface with fall from peak to residual strength. In the case of avalanche formation, a stress or strain concentration in terms of a macroscopic imperfection within a weak layer can initiate relative sliding within weak layer as described by *Bažant et al.* [2003] and suggested by *Palmer and Rice* [1973].

2.2. Influence of Column Length L_0

[10] *Gauthier and Jamieson* [2008] reported 3 types of test results. Most of the tests, they called CRL (for critical length) in which the critical length, L, was essentially independent of column length L_0. Another type of test, they called CP (for constant proportion) in which the critical length was approximately proportional to L_0, consisted of seven sets of tests. A third type of test, they labelled VAR (for variable) in which the critical length was partly influenced by L_0, consisted of three sets of tests. In this paper, only the results of CRL tests are used for which the results are independent of L_0. The reader is referred to *Gauthier* [2007] and *Gauthier and Jamieson* [2008] for a description of the other types of test results.

3. Results From Failure and Fracture of Alpine Snow in Simple Shear

[11] When deformed in simple shear, test results show that alpine snow is a pressure sensitive, dilatant, strain-softening material [*McClung*, 1979, 1987; *Schweizer*, 1998; *McClung and Schweizer*, 1999]. The experimental test results show that when failure is achieved (a peak on a shear stress-displacement curve) alpine snow is in a dilatant state whether the sample simply fails and slowly softens after the peak or whether the sample fractures and collapses or settles rapidly once the peak is achieved [*McClung*, 2007c]. Figures 3a and 3b are an example for which fracture has taken place at peak stress for fine grained, faceted snow deformed in direct simple shear as described by *McClung* [1977]. The horizontal displacement rate for this example is about 0.1 mm/min. Faceted snow is an important weak layer form which is very common in human triggered avalanche failure layers. This example shows that the characteristic mean displacement over which rapid softening takes place in a fracture experiment is of the order $\overline{\delta} = 0.1$ mm. This value is similar to results in tension fracture experiments on alpine snow [*McClung and Schweizer*, 2006] and concrete [*Bažant and Planas*, 1998, p. 180]. *McClung* [2007c] present more data in relation to this important scale for softening and fracture for alpine snow. Slow strain-softening failures without fracture typically show displacements over which softening takes place an order of magnitude above this value, i.e., $\overline{\delta} = 1$ mm or more [*McClung*, 1977]. This result is of immense importance since the size of the fracture process zone is determined mostly by the material parameter $\overline{\delta}$ relatively independent of the size of the snow slab [*Palmer and Rice*, 1973]. In addition, the fracture tests exhibit much more severe strain softening (drop from peak to residual) compared with results from slow tests.

[12] Another important effect for shear fracture in shear frame tests as opposed to slow softening failure or rapid softening fracture is that the pressure sensitivity is greatly reduced. Slow, strain-softening tests on faceted snow [*McClung*, 2007c; *McClung*, 2007c] show that peak friction angles are typically in the range $50° < \phi < 70°$ for either slow failure and softening or for slow failure followed by fracture and rapid softening accompanied by collapse. Figure 4 shows a peak failure envelope for the faceted snow similar to that in Figures 3a and 3b. The slope of the curve gives a peak friction angle of approximately 70°. These peak friction angles are higher than slope angles for which avalanches release [*McClung and Schaerer*, 2006] which suggests that imperfections or strain and stress

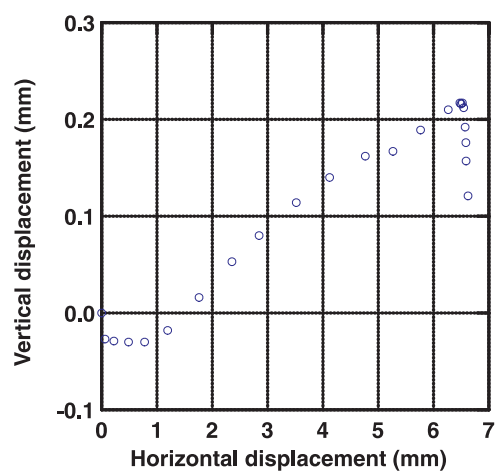

Figure 3b. Vertical displacement versus horizontal displacement for the sample in Figure 3a. The graphs show that fracture takes place during a dilatant state with collapse following failure at peak stress. Horizontal displacement following fracture at peak stress is of the order of 0.2 mm. Horizontal displacement rate is 0.1 mm/min. The sample size is 11.5 cm diameter with a height of 2 cm.

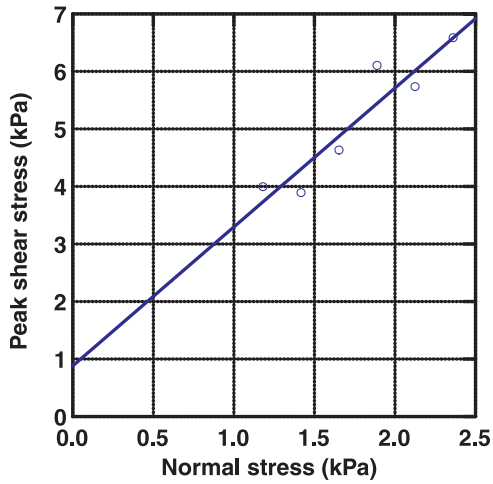

Figure 4. Failure envelope for six samples similar to Figures 3a and 3b with peak shear stress plotted versus applied normal load. The data suggest a peak friction angle (from the slope of the curve) near to 70°.

concentrators in weak layers are involved in the initiation of avalanches [*McClung*, 1987]. Fracture tests performed rapidly by *Jamieson* [1995] with a shear frame by applying weights on top of the frame suggest friction angles $\phi \sim 5°–10°$ during fracturing for faceted snow and surface hoar. These latter values are utilized in the model developed below to interpret the field tests described in section 2.

[13] Taken together, these results show that implied mechanical behavior including pressure sensitivity under failure with slow softening is greatly different for shear frame tests than when rapid softening takes place following fracture in a dilatant state at peak stress. Fracture implies very short characteristic displacement during softening. and the shear frame tests indicate much less pressure sensitivity (i.e., much lower friction angle) than in slow direct simple shear tests. For the model below, the most important characteristics are the low-pressure sensitivity (low values of ϕ) and the characteristic displacement of order 0.1 mm during fracturing.

4. One-Dimensional Model for Quasi-Brittle Fracture Initiation With Finite Fracture Process Zone

[14] The model presented by *Palmer and Rice* [1973] for initiation of shear fracture on a slope provides the basic starting point. The model was applied to avalanche failures by *McClung* [1979, 1981] and *Bažant et al.* [2003]. The basis of the model of *Palmer and Rice* [1973] is that failure of a strain-softening material in a shear band underneath a slab results in fracture once a critical length is achieved. An important assumption which is retained in the new model presented below is that the dominant deformations take place in the weak layer (sliding layer) as opposed to the slab. The fracture process zone over which strain softening takes place is considered to be of finite size. However, the implications of the model of *Palmer and Rice* [1973] are such that the overall length of the band must be greater than or equal to characteristic size[*Bažant et al.*, 2003]. Also, the length of the fracture process zone (FPZ) must be less than in order to form correspondence with the analogy to linear elastic fracture mechanics (LEFM). Thus, it was assumed that $\omega \ll L$ in previous models.

[15] The test data summarized below (Table 2) show that the ratio L/D is often less than one. In Appendix A, I have summarized the scaling of L/D and I have provided approximate estimates of for the new model below which is developed for $\omega \leq L$ to replace the assumption of small FPZ ($\omega \ll L$). Even though two dimensional solutions are required [*Bažant et al.*, 2003] for best accuracy, such models involve assumptions about mechanical behavior and properties which are unknown for alpine snow. The uncertainties involved in 2-D modelling would negate the greater accuracy sought. Therefore, one dimensional modelling is retained below.

[16] Estimates of the critical lengths for alpine snow are in the range of several 10s of cm. [*McClung and Schweizer*, 1999]. The length-scale data in Table 2 suggest that the original model of *Palmer and Rice* [1973] should be modified such that a finite FPZ may be assumed. In the model below, therefore, I assume that $\omega < L$ to derive a propagation condition for specifying the critical length scaled with D, L/D. It may be noted that if $\omega \geq L$ then layer failure is achieved when peak shear strength is mobilized all along the band. From the concepts developed by *Palmer and Rice* [1973], fracture may ensue at applied shear stress well below peak stress for long bands, $L/D \gg 1$. From the values in Table 2, it can be expected that the applied shear stress is near but below peak nearly all along the band since the bands lengths are fairly short when scaled with D and I take this assumption in the model below.

[17] The model developed below is expected to be applicable approximately to the fracture data reported above and also to dry snow slab avalanche initiation. The fracture mode is taken as mode II, inplane shear deformation. Even though avalanche shear failures spread upslope and across slope after initiation, I suggest that initiation is mostly in the upslope and/or downslope direction since the applied shear stress by slab weight is in the downslope direction and this is the same geometry used in the test data analyzed in this paper.

4.1. Model Assumptions

[18] The model is developed by considering the geometry in Figure 2 appropriate to the field test data described above. A crack is introduced within the weak layer by making a cut with a 2 mm thick snow saw upslope from the lower end of the slab. Two important effects are expected by making the cut: release of gravitational potential energy and introduction of slope parallel slip along the band. The

Table 2. Descriptive Statistics for L and L/D[a]

Forms	Sets/Number of Tests	L (Median) (m)	L (Range) (m)	L/D (Median)	L/D (Range)
NP	6/121	0.25	0.07–0.71	0.66	0.14–2.00
SH	11/177	0.37	0.19–0.95	1.15	0.47–2.52
FC	7/91	0.24	0.18–0.38	0.85	0.29–1.14
ALL	33/488	0.33	0.07–0.95	0.87	0.14–2.52

[a]Weak layer crystal forms include NP (nonpersistent), SH (surface hoar), and FC (faceted crystals).

gravitational energy per unit area released with a slope normal drop of order $\Delta y \approx 1$ mm [*Sigrist*, 2006, p. 90] is given approximately by $\rho g D(\Delta y)\cos\psi$. For median values given below, $D = 0.41$ m; $\rho = 152$ kg/m^3 and $\psi = 20°$, the energy released per unit area is about 0.6 or 1.2 N/m for a drop of 2 mm corresponding to saw blade thickness. This exceeds the mode II fracture energy, G_{II}, for avalanche weak layers (0.005–0.1 N/m) estimated by *McClung* [2007a] by at least a factor of 5. Thus, if even less than 20% of the gravitational energy is directed toward horizontal displacement during fracture, G_{II} can be exceeded. Since the initial fracture is a shear fracture in the weak layer, I suggest that a fraction of the gravitational energy released will be associated with slip in the slope parallel direction following failure at peak stress. Weak layers composed of persistent forms such as faceted crystals, surface hoar, and depth hoar are expected to have anisotropic (orthotropic) behavior, resistant to slope normal deformation and propensity for shear or slope parallel deformation when disturbed [*McClung*, 2007c]. For a granular material like snow, with typically only 20% volume fraction filled by solid material, it would be highly unlikely to make a saw cut in the weak layer without generating slip in the slope parallel direction as well as slope normal displacement. High-speed photography of field tests, as reported here, has confirmed the presence of both slope parallel and slope normal displacements [*van Herwijnen et al.*, 2008] associated with shear fracture propagation.

[19] Following failure of the material in the weak layer at peak shear stress at the tip of the band, I assume strain softening over the region of the fracture process zone with horizontal slip along the band starting from $\delta = 0$ at the band tip where peak shear strength is attained. Behind the band tip, I distinguish between two cases to describe the relation between shear stress and displacement along the band:

[20] 1. In case 1, for an infinitesimally thin band, the applied shear stress is taken as the downslope gravitational shear stress due to the weight of the slab, $\tau_0 = \tau_g = \rho g D \sin\psi$. This case corresponds to small weak layer thickness d_0 and it may be applicable to some cases of avalanche release. Case 1, for the present model, amounts to application of initial stresses generated by body force per unit volume of magnitude, τ_g/D, all along the band. This case applies to a very thin band with no slope normal deformation during stress relief. This is an approximation since near the tip of the band a constant relationship is not expected to hold exactly. Energy release per unit area as the band extends by Δx is given by $\tau_g \Delta x$ due to slab weight.

[21] 2. In case 2, for examples in which a cut is made, such as the experiments described here, or where failure is within a weak layer of finite thickness, d_0, on the order of 1 cm or so, I assume that slope normal displacement in the weak layer (e.g., Figure 1a) releases gravitational energy which is also accompanied by horizontal slip and effective applied shear stress along the band. For a weak layer of finite thickness or when a cut is made, I assume that $\tau_0 = \mu_0 \rho g D \cos\psi = \mu_0 \sigma_N$ where μ_0 is a dimensionless coefficient. The horizontal slip along the block is expected to produce tensile stress at and near the tip of the shear band. Typical values for horizontal deformation, $\overline{\delta}$, during snow fracturing are on the order of about 0.1 mm from laboratory measurements as shown above.

[22] Case 2, amounts to application of initial stresses as a proportion of the slope normal body force per unit volume σ_N/D all along the band. This case accounts for initial stresses released by vertical and horizontal deformation in a thick weak layer by collapse (e.g., by failure of relatively thick layers of persistent forms) or by introduction of a saw cut, as with the experiments. As with case 1, this case is an approximation since near the tip of the band (within the FPZ) since it is unlikely that a constant relationship would hold exactly. Energy release per unit area as the band extends by Δx is given by $\mu_0 \sigma_N \Delta x$ due to slab weight. Case 2 provides the suggestion that given the same slab and weak layer properties, the energy release is higher for lower slope angles than for higher slope angles. It also provides an explanation for propagation when $\psi = 0°$ as observed by *Gauthier and Jamieson* [2008] and as illustrated in Figure 1b. The field data presented below show shorter critical lengths for slopes of lower angle to support the model assumption.

[23] For case 2, it can be expected that slope normal deformation in the weak layer may result in slab bending with a compressive zone at the bottom of the slab over the region of the FPZ where slope normal deformation is taking place. In addition, there may be shear deformation by rotations within the slab. These effects are ignored in the present model but they represent work that must be done to deform the slab as the cut is made in an experiment.

[24] Since case 1 and case 2 represent gravitational energy release through snow fracturing, there is no reason why case 1 cannot also be formulated by a dimensionless coefficient multiplied by applied normal stress as with case 2. However, there are no shear experiments available for a layer of infinitesimal thickness and so case 1 is retained as stated for correspondence with the previous models of *Palmer and Rice* [1973] and *Bažant et al.* [2003] and their direct analogy to conventional mode II fracture mechanics.

[25] For case 2, because of the low effective friction angle during fracturing, I expect that a significant portion of the available energy will be available for production of shear fracture surface at and near the tip of the band in the FPZ. From simple modelling as a pressure sensitive material, the available shear stress (traction) from initial stress on the band following fracturing at peak shear stress in a dilatant state may be estimated. The traction, without residual friction, is approximately $\tau_0 = \mu_0 \sigma_N$ where $\mu_0 = \tan\phi$ is analogous to an the effective friction coefficient during fracturing.

[26] The traction including residual friction is then $\sigma_t = \tau_0 - \tau_r$ with residual shear strength, τ_r, mobilized along the band. For case 1, $\sigma_t = \tau_g - \tau_r$. For case 2, $\sigma_t = \mu_0 \sigma_N - \tau_r = \tan(\phi)\sigma_N - \tau_r$. From the work of *Jamieson* [1995], values of are expected to be in the approximate range of 5°–25° depending on crystal form in the weak layer with the lower values expected for persistent forms (5°–10°) including faceted crystals and surface hoar. Similar values are suggested by relating horizontal and vertical displacement during simple shear fracture tests on alpine snow [*McClung*, 2007c]. Thus, it is assumed that failure occurs in a dilatant state when peak stress is achieved at the head of the FPZ with both slope parallel and slope normal deformation (collapse) occurring during fracturing over the scale of the FPZ. Figure 3a shows the stress and deformation

pattern during fracturing and collapse of facted snow as support of this assumption.

[27] The approximation of constant initial stress all along the band for both cases means that for the model below, details such as slip and traction within the FPZ will not be highly accurate. For short bands, detail within the FPZ becomes very important so that two dimensional modelling is required for good accuracy [*Bažant et al.*, 2003]. However, here the emphasis is on the propagation condition which is mostly determined by details outside the FPZ so the one dimensional approximation may be acceptable for the application sought here.

[28] Following *Palmer and Rice* [1973], I assume for simplicity that the cohesive crack model applies with δ being the relative horizontal slip between surfaces of the shear band and I take the drop from peak shear strength, τ_p to τ_r being linear in the fracture process zone, so that the mode II fracture energy is represented as $G_{II} = (\tau_p - \tau_r)\overline{\delta}$ where $\overline{\delta}$ is the mean displacement in the FPZ. Failure occurs by propagation of a slip surface (or shear band) for which relative sliding leads to reduction of strength from peak to residual within the FPZ and the traction vector at every point on the band satisfies the yield condition corresponding to a value of δ at that point. The stress field behind the tip of the band is assumed to be continued smoothly into the region ahead of the band where failure has not yet taken place with no singularities or point force regions. This assumption is appropriate for a quasi-brittle material with a finite sized FPZ compatible with the cohesive crack model. *Bažant* [2005] has outlined some of the limitations of the cohesive crack model, introduced by *Rice* [1968], which normally includes this deformation assumption. Following *Palmer and Rice* [1973], it is assumed that the snow below the weak layer is much stiffer than the slab above the weak layer so that any deformation below the weak layer is not accounted for. *McClung and Schweizer* [2006] have discussed some of these limitations with respect to the snow slab.

4.2. Model Development

[29] The model is developed with the assumptions that the dominant deformation and energy transfer is in the weak layer (or sliding layer) and stress deformation pattern within the FPZ is unchanged as the band moves or as the cut is made. The model development is for inplane shear deformation (mode II). However, the development is based on the work of *Cleary and Rice* [1974] derived for antiplane shear deformation (mode III) during deformation. The equations developed by *Cleary and Rice* [1974] for antiplane deformation may be derived from the model development here by replacing the elastic modulus with the shear modulus [$E' = (2\mu/1 - \nu) \rightarrow \mu$] where μ, ν are the elastic shear modulus and Poisson's ratio respectively. Simple extension of Cleary and Rice's model is included to contain the possibility of slope normal deformation during extension of a weak layer of finite thickness, d_0, is included in the model below as presented in section 4.1.

[30] When slope normal displacement takes place, it will also be required that slab bending may take place as well as shear deformation by rotations in the slab. Both of these will require energy input as the band extends but these terms are ignored in the present formulation.

[31] Following *Palmer and Rice* [1973] and *Rice* [1973], the deformation is considered with respect to one dimensional modelling. The coordinate system is such that x is measured from the left end of the block ($x = 0$) to the end of the cut or slip surface ($x = L$) in the direction parallel to the weak layer (Figure 1b). The x deformation is considered as $u(x) = -\delta(x)$. The weak layer slip begins with $\delta = 0$ at the tip of the band ($x = L$) increasing to $\delta = \delta_0$ at the left end of the band ($x = 0$) with a value $2\overline{\delta}$ at the end of the FPZ ($x = L - \omega$) as explained below.

[32] Initially, the stress strain relation for the slab material is taken as linear elastic, with depth averaged tensile stress being given by

$$\overline{\sigma} = E'\overline{\varepsilon} - p_0 = -E'\frac{d\delta}{dx} - p_0. \tag{1}$$

In equation (1), positive extensional strain is given by $\overline{\varepsilon} = -d\delta/dx$ since δ decreases as x increases. In equation (1), $-p_0$ represents depth averaged compressive stress (analogous to pressure) when $\overline{\varepsilon} = 0$ ahead of the band tip.

[33] The depth averaged equilibrium condition is given by

$$D\frac{d\overline{\sigma}}{dx} = \tau_0 - \tau(x), \tag{2}$$

where $\tau(x)$ is the shear stress distribution on the band. The shear stress distribution on the band may be represented in terms of δ as

$$\begin{aligned} \tau(\delta) &= \tau_r \quad \text{for} \quad \delta \geq 2\overline{\delta} \\ \tau(\delta) &= \tau_r + \frac{G_{II}}{\overline{\delta}}\left[1 - \frac{\delta}{2\overline{\delta}}\right] \quad \text{for} \quad \delta \leq 2\overline{\delta}. \end{aligned} \tag{3}$$

In equation (3), for simplicity, the stress drop from peak ($\delta = 0$) to residual ($\delta = 2\overline{\delta}$) is taken linear with δ in the FPZ with a residual value outside of the FPZ.

[34] Multiplication of equation (2) with the average extensional strain and integrating gives

$$D\int_0^x \overline{\varepsilon}\frac{d\overline{\sigma}}{dx'}dx' = -\int_0^x \tau_0\frac{d\delta}{dx'}dx' + \int_0^x \tau(x')\frac{d\delta}{dx'}dx'. \tag{4}$$

Now when $x = L$, the critical condition for extension of the band is achieved. The mean value of the longitudinal stress at the free surface is given by $\overline{\sigma}(x = 0) = 0$. Up slope and just behind the band tip, $\overline{\varepsilon} = 0$ [*Cleary and Rice*, 1974] and the mean value of the longitudinal stress is given by $\overline{\sigma}(x = L) = -p_0$. Thus, equation (4) can be expressed as

$$D\int_{\overline{\sigma}(x=0)=0}^{\overline{\sigma}(x=L)=-p_0}\left(\frac{\overline{\sigma} + p_0}{E'}\right)d\overline{\sigma} = -\int_{\delta_0}^{0}\tau_0 d\delta + \int_{\delta_0}^{0}\tau(\delta)d\delta. \tag{5}$$

Using equation (3), the propagation condition is then given by

$$\frac{Dp_0^2}{2E'} + (\tau_0 - \tau_r)\delta_0 = G_{II}. \tag{6}$$

In (6), the first term on the left represents energy per unit area from pressure relief and the second term is gravitational energy per unit area released by stresses in excess of residual. These driving terms on the left size are balanced by the mode II fracture energy within the weak layer on the right side.

[35] In order to fully develop the propagation condition, the slip, δ_0, at the end (free surface) of the band must be obtained. Integration of equation (4) over the limits from L (at the tip of the band) to x gives the following equation:

$$D\int_L^x \bar{\varepsilon}\frac{d\bar{\sigma}}{dx'}dx' = -\int_L^x \tau_0\frac{d\delta}{dx'}dx' + \int_L^x \tau(x')\frac{d\delta}{dx'}dx'. \qquad (7)$$

Upon integration, with $\delta = 0$, $\bar{\varepsilon} = 0$ at $x = L$ at the tip of the band [*Cleary and Rice*, 1974], gives the following differential equation in terms of δ at position x

$$\frac{DE'}{2}\left(\frac{d\delta}{dx}\right)^2 = \int_0^\delta [\tau(\delta) - \tau_r]d\delta - (\tau_0 - \tau_r)\delta. \qquad (8)$$

For $\delta \geq 2\bar{\delta}$, equation (8) reduces to

$$\left(\frac{d\delta}{dx}\right)^2 = C_0 - C_1\delta, \qquad (9)$$

where $C_0 = 2G_{II}/DE'$; $C_1 = 2(\tau_0 - \tau_r)/DE'$.

[36] Solution of (9) gives

$$x = \frac{2}{C_1}\sqrt{C_0 - C_1\delta} - \frac{2}{C_1}\sqrt{C_0 - C_1(2\bar{\delta})} + (L - \omega) \qquad \delta \geq 2\bar{\delta}. \qquad (10)$$

Now if $x = 0$, then $\delta = \delta_0$ and after some algebra, the propagation condition is obtained as

$$\left[\sigma_t\left(1 - \frac{\omega}{L}\right)\frac{L}{D} + p_0\right]\sqrt{\frac{D}{2}} = \sqrt{E'}\sqrt{G_{II}\left(1 - \frac{2\sigma_t\bar{\delta}}{G_{II}}\right)} \qquad \omega \leq L, \qquad (11)$$

where $\sigma_t = \mu_0\sigma_N - \tau_r$ to emphasize the dependence on normal stress during failure of layers of finite thickness or $\sigma_t = \tau_g - \tau_r$ for an infinitesimally thin layer. Equation (11) is subject to the constraint that $2\sigma\bar{\delta}/G_{II} < 1$.

[37] Equation (11) may be expressed in a form analogous to *Irwin's* [1958] equation relating an effective fracture energy, G_{II}^*, and an effective critical stress intensity factor, K_{IIc}^*, such that

$$G_{II}^* = G_{II}\left(1 - \frac{2\sigma_t\bar{\delta}}{G_{II}}\right); \; K_{IIc}^* = \left[\sigma_t\left(1 - \frac{\omega}{L}\right)\frac{L}{D} + p_0\right]\sqrt{\frac{D}{2}}. \qquad (12)$$

From equation (12), $K_{IIc}^* = \sqrt{E'G_{II}^*}$ analogous to *Irwin*'s [1958] relation for fracture toughness. It is important that G_{II}^*; K_{IIc}^* are not equated to G_{II}; K_{IIc} which are fracture energy and fracture toughness and terms reserved for linear elastic fracture mechanics in which the FPZ is taken as infinitesimal instead of finite as is appropriate for alpine snow.

[38] For the special case of $\omega/L \ll 1$ and $\sigma_t\bar{\delta}/G_{II} \ll 1$ equation (12) reduces to the expression given by *Palmer and Rice* [1973] and *Rice* [1973] for the same geometry when $\sigma_t = \tau_g - \tau_r = \rho g D\sin\psi - \tau_r$.

[39] Solution of equation (8) for slip in the FPZ gives

$$\delta = 2\bar{\delta}\left[\frac{G_{II}/\bar{\delta} - \sigma_t}{G_{II}/\bar{\delta}}\right]\left\{1 - \cos\left[(L - x)\sqrt{\frac{G_{II}}{2DE'\bar{\delta}^2}}\right]\right\} \qquad \delta \leq 2\bar{\delta}. \qquad (13)$$

For equation (13), it may be verified that $\delta = 0$, $\bar{\varepsilon} = -d\delta/dx = 0$ at $x = L$.With $\delta = 2\bar{\delta}$; $x = L - \omega$, the FPZ size is estimated as

$$\omega = 2\bar{\delta}\sqrt{\frac{2D\bar{\delta}^2E'}{G_{II}}}\cos^{-1}\left[\left(1 - \frac{1}{C_2}\right)\right] = \sqrt{\frac{2D\bar{\delta}^2E'}{G_{II}}}\left[\frac{\pi}{2} + \sin^{-1}\left(\frac{\sigma_t}{G_{II}/\bar{\delta} - \sigma_t}\right)\right], \qquad (14)$$

where $C_2 = [(G_{II}/\bar{\delta} - \sigma_t)/(G_{II}/\bar{\delta})]$.

[40] The size of the FPZ from equation (14) is considered in Appendix A where it is suggested that equation (14) is not very accurate. One reason is the approximation of constant initial stress, σ_t, released all along the band. Other reasons include the limitations of the standard cohesive crack model as discussed by *Bažant* [2005, pp. 179–182] and the simple linear slip relation of equation (3). In Appendix A, approximate scaling of ω with weak layer grain size is given and ω is related to propagation length L.

5. Estimates of Critical Length Ratio From the One-Dimensional Model

[41] Consider equation (11) written in the nondimensional form

$$\frac{\tau_0\left(1 - \frac{\omega}{L}\right) + p_0\frac{D}{L} - \tau_r\left(1 - \frac{\omega}{L}\right)}{\tau_p - \tau_r} = \sqrt{\frac{2E'\bar{\delta}^2}{DG_{II}}}\sqrt{1 - \frac{2\sigma_t\bar{\delta}}{G_{II}}}\left(\frac{D}{L}\right). \qquad (15)$$

In equation (15), the first two terms in the numerator on the left side represent the average shear stress on the band due to gravitational loading and the lateral pressure. The maximum value of the average shear stress is τ_p. For short bands, when ω is comparable to L, failure of the layer will occur when the applied shear loads are near τ_p. *Palmer and Rice* [1973] showed that long bands may satisfy the propagation condition when the applied loads are well below peak. If the pressure term is small, it is easy to see that the ratio on the left side of equation (15) is less than one. Considering the concepts outlined by *Palmer and Rice* [1973] and *Rice* [1973], it is suggested that the ratio in (15) is less than or equal to 1 so that an inequality results for the right hand side and

$$\frac{L}{D} \geq \sqrt{\frac{2E'\bar{\delta}^2}{G_{II}D}}\sqrt{1 - \frac{2\sigma_t\bar{\delta}}{G_{II}}}. \qquad (16)$$

For the experiments, it is possible that ω may be, as long, or longer than the block length L. In that case, equation (12) may be applied over the length of the block and the pressure is given from $\overline{\sigma}(x = 0) = 0$ or $p_0 = -E'(d\delta/dx)_{x=0}$. Solution gives an expression for L/D as

$$\frac{L}{D} = \sqrt{\frac{2E'\overline{\delta}^2}{DG_{II}}}\sin^{-1}(\beta), \tag{17}$$

where $\beta = p_0\sqrt{D/2E'G_{II}}[1/(1 - \sigma_t\overline{\delta}/G_{II})]$.

[42] Equation (16), derived for $\omega < L$, may be compared with equation (17) derived for the case when $\omega > L$. The leading square root radical on the right side is the same for both cases. Given that the numerator and denominator of β must both be positive, I suggest that $0 < \sin^{-1}(\beta) < \pi/2$ so the estimates of (14) and (17) should be of the same order. However, since the multiplier on the leading square root radical is less than 1 for equation (16) and it may as large as $\pi/2$ in equation (17), it is possible that equation (17) may yield slightly higher values for L/D. The model here, combined with the data from the field and laboratory experiments, has too much uncertainty in predictions to detect the differences. The formulation in equation (17) will not apply for avalanche initiation since $p_0 \rightarrow 0$ in that case. For the latter, from equation (15), if $\tau_0 \rightarrow \tau_p$, expression (16) holds since the ratio on the left side is less than one for the model.

6. Size Effect Predictions on *L*

[43] Expression (16) is considered of fundamental practical importance. It is evident that for short bands but where $\omega \leq L$, an equality rather than an inequality may apply approximately. In addition, expression (15) contains the following two important, but related, size effects in relation to the critical length ratio L/D:

[44] 1. The ratio $L/D \propto 1/\sqrt{D}$ so that thicker slabs imply shorter critical length ratios, for the same mechanical properties, slope parameters and geometrically similar slabs. *McClung* [2005] provides the argument that dry snow slabs are geometrically similar. Alternatively, $L \propto \sqrt{D}$. The restriction of the same mechanical properties and slope parameters is very important since the parameters in equation (16) are related and correlated so that statistical correlations without taking this restriction will be unreliable. In fact, comparison with field data below suggests that the proportionality $L \propto \sqrt{D}$ is a second-order effect at best.

[45] 2. There is a normal stress effect under the second square root radical on the right. Higher normal stress associated with thicker slabs, for weak layers of finite thickness, implies shorter critical length ratio. I show this effect below from field data. The data presented below exhibit highly significant negative correlation of L and L/D on normal stress as the model suggests. Expression (16) also contains slope angle dependence on the left side for case 2, since $\sigma_t = \mu_0\sigma_N - \tau_r$ where $\sigma_N = \rho g D\cos\psi$. For the same slab parameters and mechanical properties, expression (15) predicts shorter critical lengths for lower slope angles as shown by *Gauthier* [2007] from tests on 24 January 2006 and my own tests in March 2008 presented below. Variations in effective slab modulus E' and fracture properties ($\overline{\delta}$, G_{II}) also may have significant effects on the value of L/D including viscoelastic effects and temperature as discussed below.

[46] The same size effect concepts apply to the critical length ratio for avalanches. I considered [*McClung*, 1979, 1981] the case for plane strain failure of a slab (without a free surface) in mode II. In that case, $p_0 \rightarrow 0$, equations (10) and (14) apply and inequality (16) remains. *Bažant et al.* [2003] considered a fracture mechanical size effect on nominal shear strength for the snow slab. I have given a similar formulation in Appendix B for the one dimensional model given here. However, the size effect on critical length ratio L/D (or L) is expected to be of much greater practical significance since critical lengths are easily measurable in the field and they depend on slab and weak layer properties which are important in snow slab instability evaluation.

7. Data Characteristics

[47] Two data sets are presented in this paper on the basis of the fracture field tests described above. First, the results of 488 tests summarizing median values of cut lengths from 33 different weak layers described as CRL or tests for which critical lengths were measured. From this data set, the basic characteristics of L and L/D are presented and a comparison with the model is presented for median values of parameter input. Since the data consist of 33 weak layers with different slab properties and slope characteristics, the important assumption of similar slab mechanical properties and slope angles is violated. Thus, a statistical and correlation analysis cannot yield useful results for dependence on the important variables including slope normal stress, σ_N, slope angle, ψ, and dependence on slab modulus E' and D. As an example, rank correlation between L and D gave Spearman correlation coefficient $R_s = 0.41$ for the 33 layers which is highly significant ($p \approx 0.01$) and one might be tempted to conclude that the size effect described above is exhibited. However, rank correlation of L/E' with D gave $R_s = -0.03$ which is not close to significant. This analysis suggests that the former correlation is due to the modulus which is related to D and the data set violates the condition of similar mechanical properties and slab characteristics.

[48] In order to illustrate slope angle, normal stress and size effects, a second data set collected in March 2008 is then presented with 40 measurements made on the same weak layer of surface hoar. This data set clearly illustrates the dependence of slope angle, normal stress and slab modulus as implied by the theory. The data set allows some conclusions that the size effect described above, $L \propto \sqrt{D}$ is displayed but only as a second-order effect.

7.1. Data From 33 Different Weak Layers

[49] The results consist of 488 tests which are summarized in 33 different weak layers (or sets of tests) in this paper for an average of about 15 tests in each layer or set. The weak layers consist of three general types: nonpersistent forms (6 sets, 121 tests), surface hoar (11 sets, 177 tests) and facets (7 sets, 91 tests), and 6 sets (99 test) with unreported crystal forms. Surface hoar and facets are called persistent forms since they can persist for a long time in the snow pack and they are especially dangerous for back country travellers and a prime cause of accidents and deaths.

Table 3. Summary Descriptive Statistics[a]

Forms	Sets/Number of Tests	Median Grain Size (mm)	Median Slab Density (kg/m^3)	Slab Density (Range) (kg/m^3)	Median Normal Stress (kPa)	Normal Stress (Range) (kPa)
NP	6/121	1.5	140	85–194	0.46	0.18–1.26
SH	11/177	2	155	134–213	0.61	0.23–1.02
FC	7/91	2	233	173–266	0.51	0.41–2.97
ALL	33/488	N/A	152	85–266	0.61	0.18–2.97

[a]Weak layer median grain size (mm), median slab density, range of slab density, and calculated normal stress on the weak layer. The normal stress is calculated as $\sigma_N = \rho g D \cos(\psi)$, where ρ, g, and ψ are mean slab density, magnitude of acceleration due to gravity, and slope angle, respectively.

Nonpersistent forms are typically found in new snow or the early stages of metamorphism (e.g., decomposing and fragmented forms) and they generally gain strength more rapidly than persistent forms. See *McClung and Schaerer* [2006, pp. 67–68] for further description and comparison of persistent and nonpersistent forms. The results described below are denoted by the abbreviations: FC, faceted crystals; SH, surface hoar; NP, nonpersistent forms; ALL, all forms. Tables 2 and 3 contain some important summary descriptive statistics from the data for all 33 sets of tests. Tables 2 and 3 below pertain to snow with the weak layer being dry. One set of tests from 5 April 2006 was deemed to have moist snow in the weak layer and it is omitted from these Tables 2 and 3. This case is discussed later in section 7.1 which deals with temperature effects.

[50] From Table 2, the median values of L/D are of order 1,as predicted by the one-dimensional size effect law of *Bažant et al.* [2003]. However, there are wide variations and numerous values below 1. Figure 5 shows a probability plot of the values of this important ratio. The ordinate is of logarithmic scale so the plot suggests that the data follow a log normal probability density function over most of the data range. A Kolmogorov-Smirnov (K-S) goodness of fit test was performed for $\ln(L/D)$ compared to a normal distribution giving a maximum difference statistic of 0.126 for the 33 sets of tests and two-tail probability of 0.672 indicating good evidence that the distribution of L/D is log normal. The two-tail probability for L/D analyzed for normal dependence is 0.164 with maximum difference statistic of 0.195 which shows that log normal dependence is preferred for the 33 sets of 488 CRL tests. For the critical length L, the two-tailed probabilities are 0.422 for log normal dependence and 0.181 for normal dependence. Together, the results suggest that log normal dependence for L/D and L based on the goodness of fit results and probability plots.

[51] The ratio L/D is fundamental in the theory presented above and from the predictions of *Bažant et al.* [2003]. Also, for practical applications the ratio L/D is expected to be more important than the critical length L. The lower the ratio L/D, the more unstable and more dangerous is the snow pack. A short critical length, L, paired with a deep snow pack implies an unstable snow pack combined with a deep slab which implies a dangerous situation. A measurement of short critical length implies only an unstable snow pack without the potential size of the avalanche expected taken into account. *McClung* [2008] has given estimates of how avalanche volume and destructive potential increase as D increases.

[52] Table 3 contains information on median grain size in the weak layer and density in the slab/block. The grain size information is used in Appendix A to estimate the scale of the FPZ (length of ω) with median grain size. The slab density is used to estimate the modulus of the slab in comparisons below.

[53] The median value of slab depth, D, is 0.41 m (33 sets/488 tests) with a range of 0.14–1.30 m. This range covers a broad range of avalanche applications [*McClung and Schaerer*, 2006]. The data for D follow a log normal probability density function. A K-S goodness of fit test for D compared to a log normal distribution gave a maximum difference statistic of 0.123 with two-tail probability of 0.698.

7.2. Comparison With Field Measured Lengths Including Viscoelastic and Temperature Effects for the Data Set of 33 Weak Layers

[54] *Palmer and Rice* [1973], *Rice* [1973], and *Bažant* [2005] suggest that the scale of the fracture process zone is a characteristic length which is a material property. According to *Bažant* [2005], such a length implies a characteristic time $t_c = \omega/V$ where V is the speed at which stress alterations take place. For the experiments reported here, the cut speed is estimated at about 0.2 m/s [*Gauthier*, 2007] and the FPZ is estimated as one to several tens of cm which suggests that the characteristic time is of order 1 s or a frequency of about 1 Hz. For such slow deformation in alpine snow, there will be viscous effects [*McClung*, 2007b] which imply temperature effects. *Palmer and Rice* [1973] and *Rice* [1973] showed that the model concepts apply for viscoelastic slab

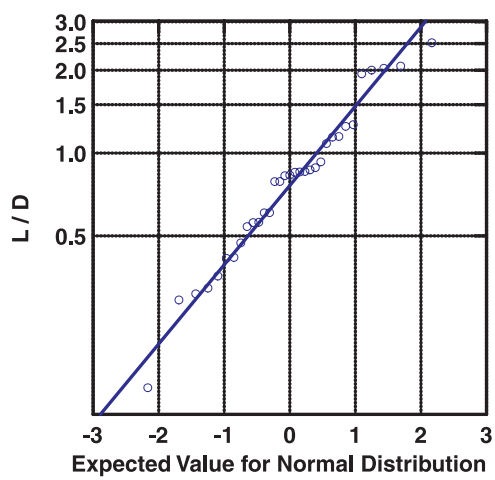

Figure 5. Probability plot for experimental values of the median of L/D for 33 weak layers representing 488 tests. The plot suggests that the ratio follows a log normal probability function.

deformation provided that a viscoelastic slab modulus is chosen compatible with the speed of stress alterations. For a frequency of 1 Hz, I provided an estimate of the viscoelastic modulus of alpine snow as a function of density. The effective shear modulus is estimated [*McClung*, 2007b] on the basis of tests by *Camponovo and Schweizer* [2001]

$$\log_{10}[\mu(f)] = 5.58 + 0.00857(\rho - 215) \quad \mathrm{Pa}(f = 1\ \mathrm{Hz}). \quad (18)$$

In all calculations below, I assume E' (1 Hz) = 2.5 μ (1 Hz) with constant Poisson's ratio of 0.2 for comparison with the field data.

[55] I determined a range of values for G_{II} [*McClung*, 2007a] appropriate for avalanche weak layers as 0.005–0.1 N/m with a median value of about 0.02 N/m. With G_{II} = 0.02 N/m and data in Table 1 (the median density 152 kg/m^3, the median value of D = 0.41 m and $\overline{\delta}$ = 0.1 mm), the modulus is estimated as E' = 0.29 MPa. The critical length ratio from (16) is roughly 0.89 which compares with the median value from the data from Table 2 of 0.89 and the calculated mean value of 0.93 ± 0.21. The theoretical value is determined by ignoring the normal stress term on the right side of equation (16). The estimated median normal stress in this case is about 0.61 kPa. From the data, the normal stress term becomes highly significant at about 1 kPa. The comparisons above suggest that the model combined with fracture and strain-softening parameters contains reasonable predictions. With the variations of the parameters (E', G_{II}, $\overline{\delta}$, D, σ_t), it is straight forward to show that the ranges of L/D in Table 1 are explainable.

[56] From Tables 2 and 3, the lowest value L/D = 0.14 comes from data with the lowest slab density (ρ = 85 kg/m^3) and I suggest the low value is mostly due to low effective shear modulus. In fact, the density in this case is so low that equation (18) would not be expected to be accurate at all since it is based on extrapolation of experimental results from higher-density snow. Using the data above for this case with equation (18) and slab depth 0.51 m, gives a ratio of 0.37 which is much higher than the measured ratio. The measured critical length was only 0.07 m in this case, by far, the lowest in the data set.

[57] Another important ratio is

$$\frac{L/D}{\sqrt{E'/D}} \geq \sqrt{\frac{2\overline{\delta}^2}{G_{II}}}\sqrt{1 - \frac{2\sigma_t\overline{\delta}}{G_{II}}} \qquad \frac{\mathrm{m}^{3/2}}{\mathrm{N}^{1/2}}. \quad (19)$$

The ratio in expression (19) has slab properties on the left side and mostly weak layer properties on the right side. From the data, the left side is evaluated with $E'(\rho)$ calculated from equation (18) for the 33 sets of tests. The calculated median value of the ratio is 0.70×10^{-3} m$^{3/2}$/N$^{1/2}$ and the mean value is $(0.95 \pm 0.21) \times 10^{-3}$ m$^{3/2}$ N$^{1/2}$. Again using, $\overline{\delta}$ = 0.1 mm; G_{II} = 0.02 N/m (ignoring the normal stress term) gives 1×10^{-3} m$^{3/2}$ N$^{1/2}$ for the right hand side, which indicates good correspondence.

7.3. Temperature Dependence

[58] Since the test data are collected for slow deformation rates, much too slow for completely brittle deformation, temperature dependence can be expected in the comparison. *Gauthier and Jamieson* [2008] did not report temperature data whereas *Sigrist* [2006] reported test temperatures from −6° to −7°C. Because of data scatter, with variations of parameters, I would not expect much temperature dependence in the data reported here. However, the effect of temperature can be roughly estimated using equation (16) from known temperature dependence of snow properties from simple shear experiments. It was shown by *Schweizer* [1998] that peak shear stress decreases by about 20% as the temperature increases from −15° to about −2°C whereas the tangent modulus, μ, as determined by simple shear experiments decreases by a factor of 3 over the same temperature range [*McClung and Schaerer*, 2006, p. 86]. Thus, I expect the largest effect will be on the effective shear modulus. Writing, the propagation condition analogous to *Irwin*'s [1958] relation gives

$$K^*_{IIc} = \sqrt{E' G^*_{IIc}}. \quad (20)$$

This suggests that slab warming from −15° to −2°C can decrease the effective fracture toughness by a factor of $\sqrt{3}$ by reduction in the modulus.

[59] Warming is also expected to increase the fracture energy if warming reaches the weak layer under the slab. However, this effect is expected to be much smaller than the modulus effect, provided the weak layer remains dry. *Gauthier and Jamieson* [2008] reported a critical length ratio L/D = 7.5 on 5 April 2006. This is an extreme outlier with respect to the data in Table 1. They did not report temperature data. However, air temperature records from Mount Fidelity, British Columbia, where the tests were conducted, show temperatures above freezing all day in the area. With a slab thickness of only 0.12 m, it is highly likely that temperatures within the weak layer approached or reached the melt point to greatly increase the fracture energy.

[60] The combination of slab warming, without the warming affecting the weak layer, has been noticed by avalanche forecasters performing avalanche control with explosives. Optimal effects of explosive control are achieved when the slab has warmed but warming has not yet reached the weak layer. Once the weak layer becomes moist, explosives are generally not effective in releasing avalanches. The same combination can also explain temperature releases of dry slabs [*McClung*, 1996]. Occasionally, thin dry slab avalanches release within minutes after the sun strikes the slopes in the morning. I suggest this is primarily due to reduction in effective fracture toughness by decrease in slab modulus with warming by penetration of short-wave radiation into the slab [*McClung and Schaerer*, 2006].

[61] In general, it may be said that slab warming should increase the snow pack instability by reducing the effective fracture toughness. However, should warming increase to the point where the weak layer becomes moist, the effective fracture energy may greatly increase to work against slab instability. Since both fracture energy and fracture toughness are theoretically brittle (e.g., elastic) material properties by definition, they are expected to be largely temperature independent for dry alpine snow as for ice [*McClung*, 1996]. However, the effective (viscoelastic) values will be temperature dependent. Deformation imparted by humans

Table 4. Values of L and L/D at Two Different Locations for the Same Surface Hoar Layer With 10 Tests at Each Slope Angle

L (m)		L/D			
Median	Range	Median	Range	ψ^0	Location
0.19	0.09–0.26	0.56	0.27–0.74	6.5	Rogers Pass
0.39	0.30–0.60	1.1	0.83–1.5	38	Rogers Pass
0.43	0.37–0.46	1.15	1.00–1.24	0	Kootenay Pass
0.61	0.57–0.70	2.05	1.78–2.69	32	Kootenay Pass

such as skiers or on snowmobiles will contain a viscoelastic component which implies important slab temperature dependence. It is very common to observe increased instability for skier triggering as the snow pack warms throughout the day. Thus, viscoelastic deformation is paramount for modelling skier triggering.

7.4. Data for Similar Slab Properties and the Same Weak Layer: Slope Normal, Modulus, and Dependence of L on D

[62] In March 2008, I gathered field data to assess slope angle and normal stress dependence, slab modulus, E' and dependence on D. The measurements consisted of 40 CRL tests with the same surface hoar layer. Two sets of 20 tests were conducted on the same surface hoar layer at two locations (Rogers Pass and Kootenay Pass) in British Columbia separated by more than 200 km. At each location, 10 tests were conducted on steep slopes (38°, 32°), respectively, at Rogers Pass and Kootenay Pass and 10 tests were conducted on slopes of low angle (6.5°, 0°), respectively, at Rogers Pass and Kootenay Pass.

7.4.1. Dependence of L and L/D on Slope Angle

[63] Two sample t tests and Mann Whitney tests were performed for two the groups at each location. The results showed that for L, L/E' or L/D there is a highly significant difference between the groups with shorter critical cut length on the lower angled slopes and significance $p < 0.0005$. In fact, for each set of tests, the shortest cut length on the steeper slope was longer than the longest cut length on the lower angled slope. Table 4 contains the median values and ranges for the four sets of tests.

[64] The values in Table 4 suggest dramatic slope angle dependence for the tests on surface hoar, with median values on steep slopes (>30°) for which avalanches are expected being about twice those for low angled slopes. *Gauthier and Jamieson* [2008] obtained a similar result for one set of tests performed on 24–25 January 2006: critical length was significantly shorter for $\psi = 0°$ than for $\psi = 30°$. However, the median cut lengths only differed by 6 cm and the type of snow in the weak layer was decomposing and fragmented which is not a type prone to collapse as opposed to the tests on surface hoar described above. Another set of tests performed on 8 February 2006 for the same weak layer of faceted crystals but different slab depth and density (i.e., different σ_N) and slope angles $\psi = 0°$ and $\psi = 23°$ did not show the slope angle effect. For the 8 February 2006 set of tests, the applied normal stress for the steeper slope ($\psi = 23°$) is actually slightly higher than for the flat terrain (2.7 and 2.5 kPa, respectively), and the slab thicknesses (1.30 and 0.98 m) are greatly different. Also, the slab densities (233 and 266 kg/m^3), which determine the slab elastic or viscoelastic modulus, are significantly different. I suggest that the combination of these differences prevents analysis of slope angle or normal stress effects for the 8 February tests.

7.4.2. Correlation Analysis for the Ratios L/D With E' and L/E' With D

[65] The model contains the predictions that L/D should increase with E' and the size effect prediction that L/E' should increase with D. For tests at Rogers Pass, the Spearman rank correlation coefficient, R_s for L/E' with D was 0.35 with significance $p > 0.05$ ($\psi = 6.5°$); 0.77 with $p = 0.01$ ($\psi = 38°$) and for Kootenay Pass, 0.38 with $p > 0.05$ ($\psi = 32°$). Thus, only one set of 10 tests displayed significant rank correlation suggesting that the size effect is very weak even though all test sets showed positive correlation. The reason for the weak effect is that the E' and D are connected.

[66] A similar analysis for correlation of L/D with E' gave R_s and p values as 0.87, $p = 0.005$ ($\psi = 6.5°$); 0.65, $p = 0.025$ ($\psi = 32°$) to illustrate the important effect of the modulus on increasing the ratio L/D as implied by the model. Because of the dominance of slope angle effects, it was necessary to consider variations for the same or similar slope angles to illustrate the correlations.

7.4.3. Correlation Analysis for Normal Stress and Shear Stress

[67] The model predicts that L and L/D should decrease with applied slope normal stress which is taken as $\sigma_N = \rho g D \cos\psi$. For results at Rogers Pass (20 tests), rank correlation of L and L/D gave −0.65 and −0.66 respectively. For Kootenay Pass (20 tests), the results were −0.74 and −0.79. The significance for all these results is such that $p < 0.005$. For the applied shear stress, $\tau_g = \rho g D \sin\psi$ similar results were obtained but with correlation of positive sign, and significance $p < 0.005$. The slope angle effects dominate in both of these correlation studies. However, the results in Table 4 provide the motivation for the normal stress effects in the model above.

8. Pressure Needed for Propagation

[68] Since the pressure p_0 results in energy released, it is possible that it may have an effect on band propagation for the tests. From the equation (11), the pressure is given by

$$p_0 = \sqrt{\frac{2E'}{D}}\sqrt{G_{II}\left(1 - \frac{2\sigma_t\bar{\delta}}{G_{II}}\right)} - \sigma_t\left(1 - \frac{\omega}{L}\right)\left(\frac{L}{D}\right). \tag{21}$$

Now if $\omega/L \rightarrow 1$ an upper limit inequality for the mean pressure is

$$p_0 \leq \sqrt{\frac{2E'G_{II}}{D}}\sqrt{\left(1 - \frac{2\sigma_t\bar{\delta}}{G_{II}}\right)}. \tag{22}$$

For an elastic or viscoelastic correspondence to the one dimensional depth averaged constitutive equation, an approximate expression for the pressure is [e.g., *McClung*, 1981]

$$p_0 = \frac{1}{2}\left(\frac{\upsilon}{1-\upsilon}\right)\rho g D \cos(\psi). \tag{23}$$

For comparison, I will take Poisson's ratio $\upsilon = 0.2$ as appropriate for slab material within the density range of Table 3. I will take $E'(\rho)$ from equation (18) and the median value for $G_{II} = 0.02$ N/m. This allows calculation of pressure estimates from equations (21) and (22). Calculations for the 3 sets of tests using these estimates showed that for 3 sets of tests, the pressure needed to drive the band (equation (20)) is less than the pressure released. If the normal stress term in equation (21) is included, the number of sets of tests would most likely increase for which the pressure released may drive the band. In Appendix A, it is suggested that the normal stress term could have a value as low as $\sqrt{0.1}$. At this extreme limit, the same calculations suggest that 11 of the 3 sets could have enough energy released by pressure relief to drive the band. I conclude that the energy released by relief of lateral pressure can have a significant effect for at least some of the tests.

[69] Since Poisson's ratio is expected to increase with slab density, and slab density generally increases with slab depth, the pressure released can increase with thicker slabs. Thus, as D increases, the pressure released increases not only with depth but by Poisson effects whereas the pressure to drive the band (e.g., equation (21)) decreases by two size effects so it becomes more likely that pressure released can drive the band.

[70] Equation (22) is written for either elastic or viscoelastic correspondence but it is very important that there is likely to be a large difference in pressure released for these two cases with higher values for the elastic case. It is beyond the scope of this paper, to speculate about the true pressure released when viscous effects dominate. The estimates in equation (21) may be considered as approximate maximum values much more appropriate for the elastic case.

9. Limitations

[71] The approach in this paper has been to present simple explanation and analysis applied to a problem which is fairly complex. The simplicity of a simple one-dimensional analytical model is chosen instead of the complexity of a potentially more accurate two-dimensional treatment. Extension to two dimensions would require assumptions about the failure and fracture properties of alpine snow which are presently unknown. Thus, uncertainty about the predicted results would remain. Simplicity is also used in the extension to the viscoelastic case through correspondence replacement of the slab modulus. Again, the true solution is undoubtedly more complex. *Palmer and Rice* [1973] pointed out that, properly, it is the unloading modulus which matters but there are not enough data on alpine snow to distinguish between the loading and unloading modulus considering variations with density, temperature and texture.

[72] Alpine snow is a material with large failure elements (bonds and grains of mm scale) which implies it is a quasi-brittle material with a FPZ comparable to or a significant fraction of important lengths in the problem including L and D. In addition, unlike concrete or other quasi-brittle materials, alpine snow is normally at a temperature which is greater than 90% of the homologous melt point and the volume fraction filled by solids is often around 20% or less for avalanche and snowpack instability problems. It is extremely unlikely that such a combination of properties could be modelled using LEFM as posed originally by *Griffith* [1921, 1924] in the 1920s with an infinitesimal FPZ. Even though the quasi-brittle approach applied in this paper remedies some of these difficulties, a final formulation with a proper viscoelastic treatment has still not been accomplished.

[73] A further complication for avalanche initiation is that in some important cases, slope normal deformation takes place during failure and fracture so that the conventional deformation patterns (inplane and antiplane) with only horizontal deformation during shear fracture initiation and propagation will be inadequate. In cases of layer failure of finite thickness, field observations show vertical deformation on the order of 1 mm or more during the fracture process (see Figure 1a). The modelling in this paper is perhaps the simplest method to account for possible two dimensional weak layer failure including slope normal and slope parallel deformation. Two dimensional finite element formulations could provide more insight but such would require guesses about the actual deformation pattern and considerable uncertainty would remain. The stress and deformation pattern within the FPZ for slab avalanche initiation would be extremely difficult, if not impossible, to determine accurately.

[74] Some limitations are also evident from the field tests. The sample widths are 30 cm (Figure 2) which is really not wide enough to completely satisfy plane strain conditions as assumed in the mode II propagation model. Also, as noted above, some of the tests have cut (critical) lengths which are near the end of the block, so that the free surface at the end of the block may have had an influence. To partially remedy this problem, only CRL tests were used here to eliminate any dependence on block length. In addition, since the tests are analyzed as sets of critical lengths (on average about 15 in a set), the true scatter in the test data is not apparent.

10. Conclusions and Discussion

[75] The field data suggest that the ratio L/D is in the range 0.1 to 2.5 for dry snow with median about 0.9. Thus, the median of the data approximately matches the ad hoc prediction of *Bažant et al.* [2003] the the ratio should be of order 1 or somewhat larger. However, values smaller than one are found in the field data. The median critical lengths for all the tests are around 30 cm from Table 2 with variation from about 0.1 m to 1 m. It is not surprising to find such variations since, in reality, each weak layer and slab consists of snow with a different combination of crystal forms and size.

[76] If snow is taken as a quasi-brittle material, the data and information suggest that fractures initiate from finite, but small, regions on the order of 1 to several 10s of cm as suggested by *McClung and Schweizer* [1999]. For practical considerations, section 6 on size effects is of primary importance. For snow slab instability evaluation, the important quantities are the critical length, L, or the ratio L/D and how these may vary with slab thickness, fracture properties and viscoelastic effects including temperature. The suggestion of small, but finite sizes, has very important implications for forecasting and decision making for backcountry travel in avalanche terrain. Such small regions

under a slab would be nearly impossible to locate. Similarly, it would be virtually impossible to measure their properties. Thus, from a fracture test, such as described in this paper or by *Sigrist* [2006] and *Gauthier and Jamieson* [2008], one can only hope to get a general idea about the state of instability not about what might be the weakest point (or worst case).

[77] For snow slab avalanche instability evaluation there are, in fact, two related types of sample size effects which of importance: 1. the fracture mechanical size effect on shear strength or L or L/D as described in the previous paragraph and 2. spatial variability of these parameters within the weak layer. From a risk perspective, spatial variability within the weak layer under a slab is of much greater importance in snowpack instability evaluation because it implies a residual uncertainty which cannot be eliminated. Avalanches will likely initiate from the weakest zone under the slab which is comparable or less than D in length. The nominal strength involved in fracture initiation within the weakest zone will then likely represent the strength for a shear sample size of nearly infinite areal extent, given that typical dimensions of snow slabs are on the order of 100 D in either slab width or downslope length [*McClung*, 2008]. Thus, I suggest that for practical applications involving snow slab instability evaluation, the fracture mechanical size effects discussed in the first paragraph of section 6, can help to interpret experimental results at a site. However, the problem of spatial variability and unknown locations of the weakest zones within the weak layer will still remain. Thus, in general, no definitive answer will be provided by an in situ fracture test such as analyzed in this paper. This is why a holistic approach to forecasting and decisions is needed [*McClung and Schaerer*, 2006] with a basis on more than one piece of evidence, e.g., a critical length ratio L/D, from a fracture test.

[78] The model ratio L/D depends upon both slab properties (E', D, σ_t) and weak layer fracture properties (G_{II}, $\bar{\delta}$) which must be important in slab instability evaluation. The simple model presented contains two important extensions over the original model of *Palmer and Rice* [1973]. These include provision so that the FPZ length ω may be as large as L (from the model of *Cleary and Rice* [1974]) and introduction of slope normal deformation during fracture through a simple model of normal stress effects. With these modifications, the model seems capable of explaining the data fairly well. For example, the normal stress and slope angle effects which appear in the data also appear in the model. In the modelling, simplicity was assumed instead of a more complex model with proper accounting for viscoelastic and two dimensional effects. This was justified on the basis that the needed experimental data on fracture properties are not available at this time. Thus, more complex modelling would involve hypotheses and guesses which would negate the expected gains from more complex modelling.

Appendix A: Model Estimate of Fracture Process Zone Size

[79] The length of the fracture process zone is expected to be a material property which may scale approximately with grain size [*Bažant and Planas*, 1998; *McClung and Schweizer*, 2006]. *McClung and Schweizer* [2006] suggested that for alpine snow, $\omega \approx 100\ x$ grain size and *Bažant and Planas* [1998] suggested that for concrete that scale is about 10 x maximum grain size. In this Appendix, I attempt estimates of ω from the simple one-dimensional model.

[80] From equation (13), the analytical estimate is

$$\omega = \sqrt{\frac{2D\bar{\delta}^2 E'}{G_{II}}}\cos^{-1}\left[\left(1-\frac{1}{C_2}\right)\right] = \sqrt{\frac{2D\bar{\delta}^2 E'}{G_{II}}}\left[\frac{\pi}{2}+\sin^{-1}\left(\frac{\sigma_t}{G_{II}/\bar{\delta}-\sigma_t}\right)\right]. \tag{A1}$$

Now if $\sigma_t \to 0$the quantity in square bracket goes to $\pi/2$. The propagation condition in equation (10) is subject to the constraint that $2\sigma_t\bar{\delta}/G_{II} < 1$. Using this expression in equation (A1) suggests that the square bracket [] $\to \pi$. Using these limits, suggests that the value of ω can be represented as

$$\omega = \sqrt{\frac{2E'\bar{\delta}^2}{G_{II}}}\sqrt{D}\{K_0(\sigma_t)\}, \tag{A2}$$

where $\pi/2 \le K_0 \le \pi$. Equation (A2) is derived entirely from slip in the FPZ so it is not expected to be highly accurate, particularly in the viscoelastic case which is used to compare with the experiments. Direct application of (A2) will overestimate the length of the FPZ. In order to be more useful, model constraints are applied consistent with the propagation condition. Substituting, equation (A2) into the inequality (15), yields

$$L \ge \omega K_0(\sigma_t)\sqrt{1-\frac{2\sigma_t\bar{\delta}}{G_{II}}}. \tag{A3}$$

Now if $\sigma_t \to 0$, then $K_0(\sigma_t) \to \pi/2$ to yield the limit, $\omega/L \le 2/\pi$ whereas the upper limit from the model is $\omega/L \le 1$.

[81] From expression (A3), let $2\sigma_t\bar{\delta}/G_{II} = 1 - \varepsilon_0$ where ε_0 is less than one. Expression (A3) may then be written

$$L \ge \omega K_0(\sigma_t)\sqrt{\varepsilon_0}. \tag{A4}$$

Thus, the upper limit ratio ω/L may be expressed as

$$\frac{\omega}{L} \le \frac{1}{\pi\sqrt{\varepsilon_0}}, \tag{A5}$$

which implies $\varepsilon_0 \approx 0.1$ for which $K_0 \to \pi$.

[82] Thus, some approximate upper limits on ω are given by $(2/\pi)L \le \omega \le L$. The lower of these values is probably a better estimate for the tests since, $\omega/L \to 1$ implies essentially that released pressure drives the band or crack. Table A1 relates median grain size, the range of upper limits of $\omega([(2/\pi)L; L])$, and the scale of ω defined by the ratio of ω to the median grain size as a scale in terms of number of grains, with crystal form and number of tests (and sets of tests) using median values of L from Table 1.

[83] I conclude that the model suggests the value of ω is around one to several 10s of cm for the tests which should

Table A1. Approximate Model Estimates of ω Scaled With Number of Grains in the Weak Layer[a]

Forms	Sets/Number of Tests	Median Grain Size (mm)	Range of ω (m)	Number of Grains
NP	6/121	1.5	0.19–0.30	125–200
FC	7/191	2	0.19–0.30	100–160
SH	11/177	2	0.22–0.35	110–175

[a]The number of grains is given by ω/(median grain size).

be approximately the minimum size for crack propagation. This was predicted by *McClung and Schweizer* [1999]. The FPZ scaling length compatible with the model is on the order of about 100 times the mean grain size in the weak layer. Since the volume fraction filled by solids is only about 20% for alpine snow, I suggest that the scale with respect to number of grains should be larger than for an engineering material like concrete which has much less air content. The conclusions here cannot be regarded as with high accuracy because of the simplicity of the model employed. *Bažant and Planas* [1998] suggested a scale on the order of 10 times maximum grain size for concrete in mode I.

[84] From the CRL test data, the value of L/D has least squares mean 0.92 ± 0.25 within one standard error. The CRL tests most closely match model assumptions. This is close to the prediction of *Bažant et al.* [2003] for a value of 1 or a little larger. Application of the limits above gives some approximate values

$$\frac{1}{\pi}\frac{L}{D} \leq \frac{\omega}{2D} \leq \frac{1}{2}\frac{L}{D}. \tag{A6}$$

[85] Inserting the least squares mean for L/D gives some rough values for $\omega/2D$ between 0.3 and 0.5 which is a finite size but somewhat below the ad hoc estimate of order 1 suggested by *Bažant et al.* [2003]. With the median value of $D = 0.41$ m from the tests, rough values for $\omega/2$ might be in the range 10–20 cm for the tests. Introduction of a saw cut with a blade 5 cm wide, as with the tests, can be expected to produce a stress concentration which is effective over a horizontal scale of several times the blade width (normally about 2–5 times the blade width by St. Venant's principle [*Sokolnikoff*, 1956]). Thus, the rough scaling here seems at least of the right order of magnitude for the failure process zone from the tests. Extrapolation to the avalanche case, where weak zones or imperfections [*Bažant et al.*, 2003] can introduce strain and stress concentrations, may not imply the same results.

[86] *Palmer and Rice* [1973] and *Rice* [1973] considered the size of the FPZ for the case in which the critical stress intensity factor is evaluated for a singular viscoelastic stress field with a small FPZ in relation to other length scales in the problem. From their work, assuming the cohesive crack model applies, the FPZ size is given by

$$\omega = \frac{9\pi}{32}E'(f)\frac{\overline{\delta}^2}{G_{II}}. \tag{A7}$$

For the median values in Table 2, ρ = 152 kg/m^3; E' = 0.29 MPa; (from equation (16)) and $\overline{\delta}$ = 0.1 mm; G_{II} - 0.02 N/m, as used previously for the test data, the estimate is $\omega = 0.13$ m. This value is of the same order of magnitude as the values in Table A1. In this case, the approximation of small FPZ eliminates dependence on other length scales (e.g., D) as in equation (A1) but the order of magnitude agreement is encouraging. Application of the simplest viscoelastic treatment, as done here, considering only the effects of slab modulus, suggests that the FPZ length is not a material constant but it depends on temperature and time. After rapid stress alterations such as by application of explosives, the driving term $K_{II}^2/E'(t, T)$ may increase with time or with increase in temperature by stress relaxation to reach a critical condition. Occasionally, avalanches release some time after avalanche control and viscoelastic effects may play an important role [*McClung*, 1996].

Appendix B: Size Effect Law Related to Strength Appropriate for Dry Slab Avalanches

[87] In this Appendix, I consider the size effect scaling law for the one-dimensional propagation condition analogous to the development given by *Bažant et al.* [2003] of the avalanche case $p_0 \to 0$. The propagation condition is

$$\frac{\sigma_t\left(1-\frac{\omega}{L}\right)}{\sqrt{1-\frac{2\sigma_t\overline{\delta}}{G_{II}}}} = \sqrt{2G_{II}E'}\frac{1}{\sqrt{D}}\left(\frac{D}{L}\right). \tag{B1}$$

Following *Bažant et al.* [2003], let the ratio L/D be expanded about the initial crack length a_0 in the equivalent crack approximation

$$\alpha = \frac{L}{D} = \frac{a_0}{D} + \frac{\omega}{2D} = \alpha_0 + \frac{\omega}{2D}. \tag{B2}$$

The propagation condition may be then restated

$$\frac{\sigma_t\left(1-\frac{\omega}{L}\right)}{\sqrt{1-\frac{2\sigma_t\overline{\delta}}{G_{II}}}} = \sqrt{2G_{II}E'}\frac{1}{\sqrt{D}}\frac{1}{\sqrt{\left(\alpha_0+\frac{\omega}{2D}\right)^2}}. \tag{B3}$$

Expansion of the denominator on the right in a two term Taylor series gives upon rewriting

$$\frac{\sigma_t\left(1-\frac{\omega}{L}\right)}{\sqrt{1-\frac{2\sigma_t\overline{\delta}}{G_{II}}}} = \sqrt{G_{II}E'/\alpha_0 c_f}\frac{1}{\sqrt{\left(1+\frac{D}{D_0}\right)}} = \frac{\tau_{(0)}}{\sqrt{1+\frac{D}{D_0}}}, \tag{B4}$$

where $\tau_{(0)}$; D_0 are $\sqrt{2E'G_{II}/\alpha_0\omega}$; and ω/α_0 respectively. Expansion of the denominator of the left side of (B4) in a two term Taylor series gives

$$\frac{\sigma_t\left(1-\frac{\omega}{L}\right)}{\sqrt{1-\frac{2\sigma_t\overline{\delta}}{G_{II}}}} = \sigma_t\left(1-\frac{\omega}{L}\right)\left(1+\frac{\sigma_t\overline{\delta}}{G_{II}}\right). \tag{B5}$$

However, $\overline{\delta}/G_{II}$; 0.005 for typically expected values and if $\sigma_t\overline{\delta}/G_{II} \ll 1$ then (B4) can be expressed as

$$\sigma_t = \frac{\tau_{(0)}}{\sqrt{1+\frac{D}{D_0}}}\frac{1}{\left(1-\frac{\omega}{L}\right)}. \tag{B6}$$

Equation (B6) reduces to the one dimensional size effect law of *Bažant et al.* [2003] if $\omega/L \ll 1$

$$\sigma_t = \frac{\tau_{(0)}}{\sqrt{1+\frac{D}{D_0}}}, \tag{B7}$$

with $\sigma_t = \tau_g - \tau_r$.

[88] Thus, two approximations ($\sigma_t\overline{\delta}/G_{II} \ll 1$ and $\omega/L \ll 1$) are needed to obtain correspondence with the size effect law of *Bažant et al.* [2003]. The same approximations are needed to derive the propagation condition posed by *Palmer and Rice* [1973] for the overhanging layer from the propagation condition of equation (10). The first implies low applied loads relative to peak shear stress and the second implies a very long band relative to the FPZ. Thus, both approximations imply a long band relative to other dimensions in the problem.

Notation

d_0 weak layer thickness (m).
D slab depth measured in slope normal direction (m).
$\overline{E}$ mean size of grains in weak layer (m).
E' effective Young's modulus of snow slab (Pa).
g magnitude of gravity acceleration (dimensionless).
G_{II} mode II fracture energy (N/m).
K_{II} mode II stress intensity factor (Pa(m$^{1/2}$)).
L critical length of shear fracture (m).
L_0 total length of snow block (m).
p_0 one-dimensional depth averaged stress (pressure) (Pa).
t time (s).
t_c characteristic time (s).
T temperature (°C).
V speed (m/s).
x longitudinal coordinate (m).
y slope normal coordinate (m).
α ratio (dimensionless).
δ displacement or slip along shear band (m).
$\overline{\varepsilon}$ depth averaged extensional strain (dimensionless).
μ elastic shear modulus or viscoelastic modulus if frequency dependent (Pa).
μ_0 dimensionless coefficient (dimensionless).
ρ mean snow slab density (kg/m^3).
ν Poisson's ratio (dimensionless).
$\overline{\sigma}$ depth averaged one-dimensional tensile stress (dimensionless).
σ_N slope normal stress on the weak layer (Pa).
σ_t $\sigma_t = \mu_0\sigma_N - \tau_r$ or $\sigma_t = \tau_g - \tau_r$ (Pa).
τ shear stress (Pa).
τ_g shear stress on weak layer (Pa).
τ_p peak shear stress (Pa).
τ_r residual shear stress (Pa).
τ_0 $\tau_0 = \mu_0\sigma_N$ (Pa).
ϕ peak friction angle (degrees).
ψ slope angle (degrees).
ω length of fracture process zone (m).

[89] **Acknowledgments.** This research was sponsored by Canadian Mountain Holidays, the Natural Sciences and Engineering Research Council of Canada and the University of British Columbia. I am extremely grateful for all the support.

References

Bažant, Z. P. (2005), *Scaling of Structural Strength*, 2nd ed., 327 pp., Taylor & Francis, New York.
Bažant, Z. P., and J. Planas (1998), *Fracture and Size Effect in Concrete and Other Quasibrittle Materials*, 616 pp., CRC Press, New York.
Bažant, Z. P., G. Zi, and D. McClung (2003), Size effect law and fracture mechanics of the triggering of dry snow slab avalanches, *J. Geophys. Res.*, *108*(B2), 2119, doi:10.1029/2002JB001884.
Camponovo, C., and J. Schweizer (2001), Rheological measurements of the viscoelastic properties of snow, *Ann. Glaciol.*, *32*, 44–50.
Cleary, M. P., and J. R. Rice (1974), Elementary models for the growth of slip-surfaces in progressive failure, *Rep. MRL-E91*, 65 pp., Brown Univ., Providence.
Dempsey, J. P., S. J. DeFranco, R. M. Adamson, and S. V. Mulmule (1999), Scale effects on the in-situ tensile strength and fracture of ice. Part I: Large grained freshwater ice at Spray Lakes Reservoir, Alberta, *Int. J. Fract.*, *95*, 347–366.
Gauthier, D. (2007), A practical field test for propagation and arrest in weak snowpack layers in relation to slab avalanche release, Ph.D. thesis, 302 pp., Univ. of Calgary, Calgary, Alberta, Canada.
Gauthier, D., and J. B. Jamieson (2008), Evaluation of a prototype field test for fracture and failure propagation in weak snow pack layers, *Cold Reg. Sci. Technol.*, *51*, 87–97, doi:10.1016/j.coldregions.2007.04005.
Griffith, A. A. (1921), The phenomena of rupture and flow in solids, *Philos. Trans. R. Soc. London Ser. A*, *221*, 163–197.
Griffith, A. A. (1924), The theory of rupture, paper presented at the First International Conference of Applied Mechanics, Delft, Netherlands.
Irwin, G. R. (1958), Fracture, in *Handbuch der Physik*, vol. 6, edited by W. Flügge, pp. 551–590, Springer Verlag, Berlin.
Jamieson, J. B. (1995), Avalanche prediction for persistent snow slabs, Ph.D. thesis, 258 pp., Univ. of Calgary, Calgary, Alberta, Canada.
McClung, D. M. (1977), Direct simple shear tests on snow and their relation to slab avalanche formation, *J. Glaciol.*, *19*(81), 101–109.
McClung, D. M. (1979), Shear fracture precipitated by strain-softening as a mechanism of dry slab avalanche release, *J. Geophys. Res.*, *84*(B7), 3519–3526.
McClung, D. M. (1981), Fracture mechanical models of dry slab avalanche release, *J. Geophys. Res.*, *86*(B11), 10,783–10,790.
McClung, D. M. (1987), Mechanics of snow slab failure from a geotechnical perspective, *Publ. 162*, pp. 475–508, Int. Assoc. of Hydrol. Sci., Geneva, Switzerland.
McClung, D. M. (1996), The effects of temperature on fracture in dry slab avalanche release, *J. Geophys. Res.*, *101*(B10), 21,907–21,920.
McClung, D. M. (2005), Dry slab avalanche shear fracture properties from field measurements, *J. Geophys. Res.*, *110*, F04005, doi:10.1029/2005JF000291.
McClung, D. M. (2007a), Fracture energy applicable to dry snow slab avalanche release, *Geophys. Res. Lett.*, *34*, L02503, doi:10.1029/2006GL028238.
McClung, D. M. (2007b), Dry snow slab shear fracture speeds, *Geophys. Res. Lett.*, *34*, L10502, doi:10.1029/2007GL029261.
McClung, D. M. (2007c), Fracture properties of faceted snow, *Geophys. Res. Abstr.*, *9*, 03123.
McClung, D. M. (2008), Dimensions of dry snow slab avalanches from field measurements, *J. Geophys. Res.*, *114*, F01006, doi:10.1029/2007JF000941.
McClung, D., and P. Schaerer (2006), *The Avalanche Handbook*, 3rd ed., 342 pp., Mountaineers Books, Seattle, Wash.
McClung, D. M., and J. Schweizer (1999), Skier triggering, snow temperatures and the stability index for dry-slab avalanche initiation, *J. Glaciol.*, *45*(150), 190–200.
McClung, D. M., and J. Schweizer (2006), Fracture toughness of dry snow slab avalanches from field measurements, *J. Geophys. Res.*, *111*, F04008, doi:10.1029/2005JF000403.
Palmer, A. C., and J. R. Rice (1973), The growth of slip surfaces in the progressive failure of over-consolidated clay, *Proc. Trans. R. Soc. London Ser. A*, *332*, 527–548.

Rice, J. R. (1968), Mathematical analysis in the mechanics of fracture, in *Fracture: An Advanced Treatise— Mathematical Fundamentals*, vol. 2, edited by H. Liebowitz, pp. 192–311, Academic Press, New York.

Rice, J. R. (1973), The initiation and growth of shear bands, paper presented at Symposium on the Role of Plasticity in Soil Mechanics Proccedings, pp. 263–278, Cambridge Univ., Cambridge, UK.

Schweizer, J. (1998), Laboratory experiments on shear failure of snow, *Ann. Glaciol.*, *26*, 97–102.

Sigrist, C. (2006), Measurement of fracture mechanical properties of snow and application to dry snow slab avalanche release, Ph.D. dissertation, 139 pp., Swiss Fed. Inst. of Technol., Zurich, Switzerland.

Sokolnikoff, I. S. (1956), *Mathematical Theory of Elasticity*, 2nd ed., 476 pp., McGraw-Hill, Bombay, India.

van Herwijnen, A., J. Heierli, and J. Schweizer (2008), Field studies of collapse propagation in weak show layers, paper presented at European Geosciences Union General Assembly, Eur. Geosci. Union, Vienna, 14–18 April.

D. M. McClung, Department of Geography, University of British Columbia, 1984 West Mall, Vancouver, BC V6T 1Z2, Canada. (mcclung@geog.ubc.ca)